# REPORT DOCUMENTATION PAGE

*Form Approved*
*OMB No. 0704-0188*

The public reporting burden for this collection of information is estimated to average 1 hour per response, including the time for reviewing instructions, searching existing data sources, gathering and maintaining the data needed, and completing and reviewing the collection of information. Send comments regarding this burden estimate or any other aspect of this collection of information, including suggestions for reducing the burden, to the Department of Defense, Executive Services and Communications Directorate (0704-0188). Respondents should be aware that notwithstanding any other provision of law, no person shall be subject to any penalty for failing to comply with a collection of information if it does not display a currently valid OMB control number.

**PLEASE DO NOT RETURN YOUR FORM TO THE ABOVE ORGANIZATION.**

| 1. REPORT DATE *(DD-MM-YYYY)* | 2. REPORT TYPE | 3. DATES COVERED *(From - To)* |
|---|---|---|
| 23-05-2007 | Journal Article | |

**4. TITLE AND SUBTITLE**

Remote Observation of the Spatial Variability of Surface Waves Interacting With an Estuarine Outflow

**5a. CONTRACT NUMBER**

**5b. GRANT NUMBER**

**5c. PROGRAM ELEMENT NUMBER**

PE061153N

**6. AUTHOR(S)**

Brian K, Haus, Rafael J. Ramos, Hans C. Graber, Lynn K. Shay, and Zachariah R. Hallock

**5d. PROJECT NUMBER**

**5e. TASK NUMBER**

**5f. WORK UNIT NUMBER**

73-6643-A4-5

**7. PERFORMING ORGANIZATION NAME(S) AND ADDRESS(ES)**

Naval Research Laboratory
Oceanography Division
Stennis Space Center, MS 39529-5004

**8. PERFORMING ORGANIZATION REPORT NUMBER**

NRL/JA/7330-04-24

**9. SPONSORING/MONITORING AGENCY NAME(S) AND ADDRESS(ES)**

Office of Naval Research
800 N. Quincy St.
Arlington, VA 22217-5660

**10. SPONSOR/MONITOR'S ACRONYM(S)**

ONR

**11. SPONSOR/MONITOR'S REPORT NUMBER(S)**

**12. DISTRIBUTION/AVAILABILITY STATEMENT**

Approved for public release, distribution is unlimited.

**13. SUPPLEMENTARY NOTES**

**14. ABSTRACT**

This paper explores the application of phased-array high-frequency (HF) radars to identify locations of enhanced local waveheights. Measurements of the near-surface current velocities and waveheights were obtained from HF radars deployed near the mouth of the Chesapeake Bay in the fall of 1997. The radar-derived near-surface velocities were compared with the upper bin (2-m depth ) of four upward-looking acoustic Doppler current profilers (ADCPs). The slopes of the linear correlations were close to one and the root-mean-square (rms) differences were similar to previous studies. Significant waveheight (Hs) estimates from both radars were compared with a laser height guage. The largest differences were observed during low winds due to overestimates at one of the radar stations and and during storms when the laser measurement failed. Further analysis focused on the HF radar results from the more reliable of the two sites. The rms difference bewteen this radar and the in situ sensor was 0.29 m. Synoptic observations of Hs over the Chesapeake Bay revealed regions of current-induced wave shoaling and refraction. Hs over the estuarine outflow increased between 19-50% relative to the incident Hs in light on-shore winds (~5 m/s). In stronger winds (>10 m/s), Hs also increased by up to 25% when there was a tidal outflow in the surface layer, although the near-surface currents were responding to both the wind and the ebbing tide.

**15. SUBJECT TERMS**

coastal currents, high-frequency (HF) radar, shoaling, wave refraction

| 16. SECURITY CLASSIFICATION OF: | | | 17. LIMITATION OF ABSTRACT | 18. NUMBER OF PAGES | 19a. NAME OF RESPONSIBLE PERSON |
|---|---|---|---|---|---|
| a. REPORT | b. ABSTRACT | c. THIS PAGE | | | Zachariah R. Hallock |
| Unclassified | Unclassified | Unclassified | UL | 15 | 19b. TELEPHONE NUMBER *(Include area code)* 228-688-5242 |

DISTRIBUTION STATEMENT A
Approved for Public Release
Distribution Unlimited



# Remote Observation of the Spatial Variability of Surface Waves Interacting With an Estuarine Outflow

Brian K. Haus, *Member, IEEE*, Rafael J. Ramos, Hans C. Graber, Lynn K. Shay, and Zachariah R. Hallock

***Abstract*—This paper explores the application of phased-array high-frequency (HF) radars to identify locations of enhanced local waveheights. Measurements of the near-surface current velocities and waveheights were obtained from HF radars deployed near the mouth of the Chesapeake Bay in the fall of 1997. The radar- derived near-surface velocities were compared with the upper bin (2-m depth) of four upward-looking acoustic Doppler current profilers (ADCPs). The slopes of the linear correlations were close to one and the root-mean-square (rms) differences were similar to previous studies. Significant waveheight ($Hs$) estimates from both radars were compared with a laser height gauge. The largest differences were observed during low winds due to overestimates at one of the radar stations and during storms when the laser measurement failed. Further analysis focused on the HF radar results from the more reliable of the two sites. The rms difference between this radar and the *in situ* sensor was 0.29 m. Synoptic observations of $Hs$ over the Chesapeake Bay revealed regions of current-induced wave shoaling and refraction. $Hs$ over the estuarine outflow increased between 19–50% relative to the incident $Hs$ in light onshore winds (~5 m/s). In stronger winds (>10 m/s), $Hs$ also increased by up to 25% when there was a tidal outflow in the surface layer, although the near-surface currents were responding to both the wind and the ebbing tide. $Hs$ was not enhanced when the outflow was below a thicker layer (>5 m) of wind-forced onshore flow.**

***Index Terms*—Coastal currents, high-frequency (HF) radar, shoaling, wave refraction.**

## I. Introduction

AS MANY sailors leaving a coastal inlet during an ebb tide have observed, the local waveheight often increases dramatically where the outgoing flow meets incoming waves. Estuarine outflows often exhibit regions of significant current shear, the location of which depends on discharge, tidal stage, and wind forcing. Surface waves propagating over these variable currents and topography experience both refraction and shoaling which can lead to spatially inhomogeneous waveheights.

Phased-array high-frequency (HF) radar systems offer the promise of making synoptic measurements of both currents and waveheights simultaneously over a coastal region of interest, therefore allowing the near-real-time identification of regions where enhanced waves pose a hazard to maritime activities. Furthermore, the high resolution (~1 km) surface current and wave information can provide the necessary information to incorporate into numerical models of these processes. The focus of this paper is on the first of these capabilities, the observation of regions of locally increased waveheights due to shoaling and refraction over topography and highly sheared currents.

Section II of this paper provides background information on wave refraction and shoaling over variable currents. HF radar observations of waves and currents are then discussed. The radar measurements of both currents and waves during the third Chesapeake Outflow Plume Experiment (COPE–3) are compared with available *in situ* observations to establish their accuracy. Two cases when the wind direction was opposing the ebb-tidal outflow from the Chesapeake Bay are examined in Sections III and IV. The first of these was a case with light winds (~6 m/s), while the second had winds >12 m/s. The source of the observed spatial variability of the wave field in these two situations is explored in Section IV.

### A. Wave Refraction and Shoaling

Surface waves are affected by many processes as they propagate across a shallow shelf. In particular, wave energy is dissipated by wave breaking and bottom friction [1]. The local waveheight is increased by shoaling caused by decreasing water depths. Waveheights also increase when waves are moving against an opposing current and decrease in a following current. Wave shoaling in opposing currents depends on their wavelength and direction relative to the current direction and magnitude. Focusing or divergence of wave rays by refraction can also be caused by either depth or current gradients. Because of the many processes involved, there can be significant spatial and temporal variability of waveheights in tidally dominated coastal regions.

If dissipative processes are neglected, the shoaling of normally incident surface gravity waves propagating over an opposing current and a sloping beach can be estimated using linear theory by $H_2/H_1 = \sqrt{(C_{g1} - U_1)/(C_{g2} - U_2)}$, where $H_1$ and $H_2$ are the waveheights, $C_{g1}$ and $C_{g2}$ are the wave group velocities, and $U_1$ and $U_2$ are the currents in the wave direction at two points along the wave propagation path [2]. From this expression, it can be seen that topography and currents influence

Manuscript received August 18, 2004; accepted September 27, 2005. This work was supported by the U.S. Navy, Office of Naval Research Data Remote Sensing Program under Grants N00014-96-1-1065, N00014-99-1-0057, and N00014-01-1-0186. **Associate Editor: L. R. Wyatt.**

B. K. Haus and H. C. Graber are with the Rosenstiel School of Marine and Atmospheric Science, Division of Applied Marine Physics, University of Miami, Miami, FL 33149 USA (e-mail: bhaus@rsmas. miami.edu; hgraber@rsmas. miami.edu).

R. J. Ramos was with the Rosenstiel School of Marine and Atmospheric Science, Division of Applied Marine Physics, University of Miami, Miami, FL 33149 USA. He is now with the Center for Southeastern Tropical Advanced Remote Sensing, University of Miami, Miami, FL 33149 USA (e-mail: rramos@rsmas.miami.edu).

L. K. Shay is with the Rosenstiel School of Marine and Atmospheric Science, Division of Meteorology and Physical Oceanography, University of Miami, Miami, FL 33149 USA (e-mail:nshay@rsmas.miami.edu).

Z. R. Hallock, retired, was with the Division of Physical Oceanography, Naval Research Laboratory, Stennis Space Center, MS 39529 USA (e-mail: zack.hallock@southwind.org).

Color versions of one or more of the figures in this paper are available online at http://ieeexplore.ieee.org.

Digital Object Identifier 10.1109/JOE.2006.886240

0364-9059/$20.00 © 2006 IEEE

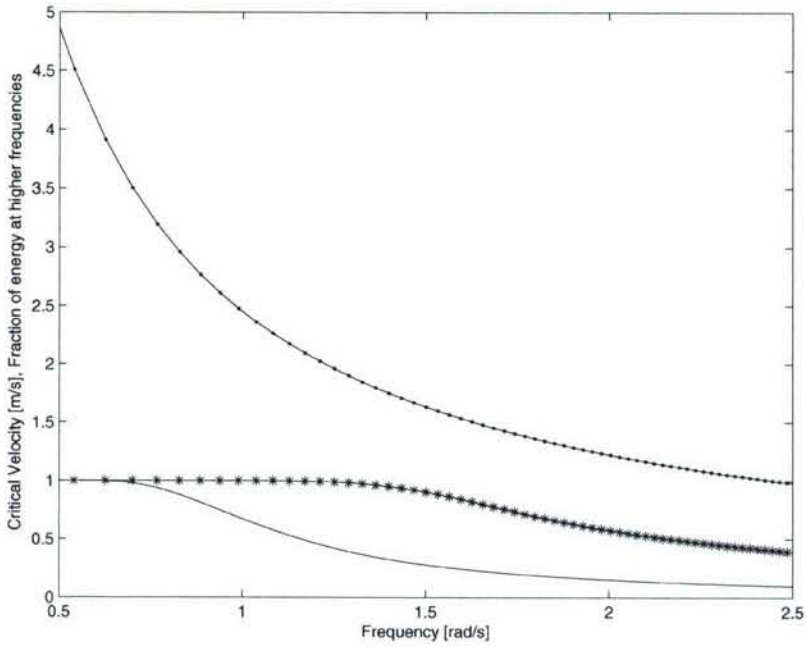


Fig. 1. (·) Critical velocity at which surface waves grow without bound related to the deep-water wave frequency. (∗) Fraction of energy of fetch limited waves with wind of 10 m/s and inverse wave age of 1.673 that occur at higher frequencies than shown [36]. (-) Energy fraction of fully developed sea at 10 m/s that occurs at higher frequencies.

the shoaling of surface waves in distinctly different ways. Small wave number ($k$) waves are most affected by topography because they "feel" the bottom before higher wave number waves. Conversely, the high wave number portion of the gravity wave spectrum is most strongly impacted by currents because the waves have lower group velocities.

The forward propagation of short gravity waves ($k > 6$) will be completely halted by currents greater than 1 m/s. This critical opposing current velocity ($U_c$) for a particular $k$ is given by $U_c = C_{g0}/2$, where $C_{g0}$ is the deep-water incident wave group velocity [3]. For fully developed seas under moderate winds, much of the wave energy will be at wave numbers such that the wave energy will not approach $U_c$ for currents less than 1.5 m/s (Fig. 1). However, for light winds, young seas, or fetch limited conditions, a significant proportion of the wave energy occurs at frequencies where unbounded growth will occur in an opposing current less than 1.5 m/s.

Because the speed of wave propagation changes as waves move across variable currents or topography, the direction of propagation of the waves will also change by Snell's Law $\mathrm{Sin}\,(\theta_1)/(C_1 - U_1) = \mathrm{Sin}\,(\theta_2)/(C_2 - U_2)$. For a uniformly sloping beach, this relationship causes waves incident at an angle to the beach to turn toward the shore-normal as the depth decreases and the waves slow down. For waves propagating obliquely into a sheared opposing current the same effect will occur. The wave rays will bend toward the normal to the streamlines in the direction of increasing current velocity. Kenyon [4] demonstrated that in cases of weakly sheared flow the ray curvature is equal to the ratio between the flow vorticity and the wave group velocity. For real coastal conditions with complicated topography and current patterns, the local waveheights can be significantly affected by the focusing and defocusing of the wave energy through refraction.

The equations governing the refraction, diffraction, shoaling, and dissipation of wave energy through bottom friction and breaking are highly nonlinear. In general, approximations to the full equations are used to estimate local wave conditions given known incident waves. Kirby and Dalrymple [5] developed a numerical solution to a parabolic approximation of the equations, which has been widely employed to model coastal wave conditions. Numerical refraction/diffraction models have been well tested in the field for relatively simple topographies and over shoals and barred beaches in laboratories [6]. However, providing sufficient spatial distribution of measurements for quantitative calibration and validation of numerical models is difficult for many coastal applications.

### B. HF Radar Measurements

HF radars can sample surface currents over large enough areas with sufficient spatial resolution to resolve tidal circulation patterns and estuarine outflow plumes. Phased-array HF radars also can observe the shoaling and refraction of surface waves over the same areas. The combination of these wave and current observations offers opportunities for real-time mapping for maritime uses as well as assimilation into or validation of numerical circulation and wave models.

Most HF radars operate in a monostatic mode of operation, in that they transmit a pulsed or continuous wave signal and then receive the backscattered signal at the same location. The time required for the signal to travel a particular distance over the ocean and return to the receiver can be precisely determined and, therefore, localizing the observations in range is easily done.

To localize the received signal in azimuth is a more complicated matter. Phased-array HF radar systems observe the in-phase ($I$) and quadrature ($Q$) signals at multiple antennas

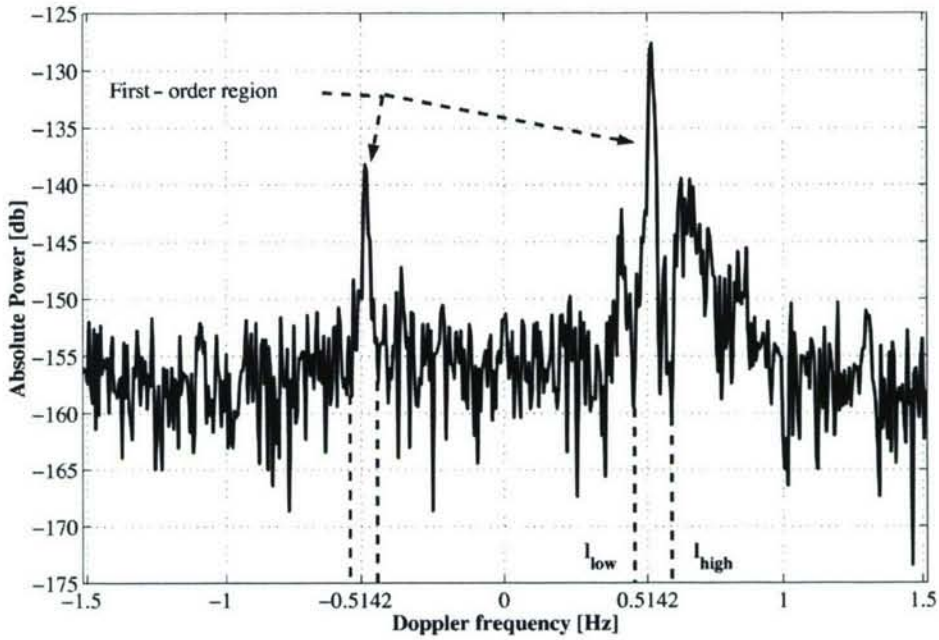


Fig. 2. Sample echo-Doppler spectrum derived from the ocean surface current radar (OSCR) HF radar operating at 25.4 MHz. First-order Bragg peaks are shown. The range of frequencies over which the second-order energy is integrated to derive waveheight is denoted by low and high.

linearly spaced at half the radar wavelength and apply predetermined phase relationships to obtain azimuthal localization. The theoretical resolution of the azimuth angle ($\theta$) is equal to the ratio between the radar wavelength ($\lambda$) and the length of the receiver array ($D$). For the phased-array system used in this paper

$$\left(\frac{\lambda}{D}\right) = \left(\frac{11.8}{88.5}\right) \longrightarrow \theta = 7.6°.$$

The backscattered signal obtained from this beamforming technique is recorded for the duration of the transmission at each range bin. Enough observations of the backscattered signal from the ocean surface are obtained during each sample period to calculate the echo Doppler spectrum (Fig. 2) from the Fourier transform of the combined $I$ and $Q$ signals.

As the number of observing antennas is increased, the signal-to-noise ratio (SNR) of the Bragg scattering signal is also increased. This renders the positions of the first-order Bragg peaks relatively insensitive to propagation path distortions of the signal for a 16-element receive array as used here. However, under some circumstances such as when the receive array is placed at a large angle to the shoreline the antenna beam pattern can become asymmetrical [7]. This has been observed to corrupt the velocity signal when the beam distortion was combined with a significant spatial in-homogeneity of the radar cross section of the ocean surface [8]. Most deployments of phased-array radars have not encountered such conditions and have not been significantly impacted by beam pattern distortions.

Direction finding techniques use compact antennas and do not construct the echo-Doppler spectrum at each range and azimuth bin. Rather they identify the direction that signals at specified frequencies are emanating from. The azimuthal resolution of HF radars using direction finding is limited by the short aperture length and they are more sensitive to antenna beam pattern distortions. In many cases, the actual beam pattern must be measured using boat mounted transponders to obtain optimal results with direction finding systems. The echo-Doppler spectrum can be constructed to make wave observations [9], but this typically requires averaging over large azimuth angles.

*1) Near-Surface Currents:* HF radar signals are preferentially scattered off waves with lengths of half the transmitted wavelength by the Bragg scattering mechanism [10]. This produces a dominant first-order peak in the echo-Doppler spectrum (Fig. 2). As the surface waves that are responsible for the Bragg scattering peaks are advected either toward or away from the radar by near-surface currents their relative speed is shifted. The surface current velocity is then determined by the offset (Doppler shift) of the first-order peaks from the zero current condition. The resolution of the radial velocity measurements is determined by the precision with which the frequency shift can be determined from the Doppler spectrum. For a pulsed system, the frequency resolution is dependent upon the pulse length and the duration of sampling which determine the total number of pulses used to derive the Doppler spectrum.

When the radial measurements from two independent stations are combined to estimate the vector current, the measurement accuracy is reduced when the radials are not orthogonal. The optimal vector resolution is, therefore, dependent upon the angle between the observations and the true current direction [11], [12]. The realized accuracy is dependent upon atmospheric conditions, sea state, and the signal properties observed at each of the receiver antennas.

HF radars have resolved the highly sheared current fields associated with the inshore edge of the Florida current [13],

small-scale instability vortices that occur in the coastal buoyancy current along the Outer Banks of North Carolina [14], and the tidal circulation patterns associated with the Chesapeake Bay outflow plume [15], [16].

*2) Surface Wave Parameters:* The echo-Doppler spectrum contains information on both the surface currents and the surface waves. In addition to the first-order Bragg resonances, a typical spectra contains significant energy at frequencies around the first-order peaks (Fig. 2). These second-order returns contain backscattered energy resulting from multiple reflections of the radar signal as well as the hydrodynamic combination of surface waves to produce Bragg scattering [17]. This second-order energy, therefore, contains information on the surface wave spectrum. This information is ideally available at every range and azimuth bin over the sampling region. However, the range of useful wave information is more limited than for current measurement because of the lower SNR associated with the second-order peaks. Phased-array HF radars can provide sufficient SNR and azimuthal resolution to allow spatial localization of wave observations.

Methods to invert the second-order contribution to the Doppler spectrum to estimate the surface wave directional spectrum have been developed by [18] and [19]. In [20], it was demonstrated that inversion methods can obtain reliable wave estimates when compared with moored buoys. These methods require that either strict bounds are placed on the frequency range of the inversion [18] or that the raw quadrature signal are collected and stored [19].

Historically, for field operations the large amount of disk storage required to archive the raw data was often difficult to manage. Archiving the Doppler spectra derived from the $I$ and $Q$ signals using fast Fourier transforms required a factor of three less storage and was often the only reasonable alternative for waveheight observation. Modern computational resources have effectively eliminated these restrictions, however, statistical parameters of the wave field such as $Hs$ are still widely used to characterize wave conditions.

Empirically based methods to derive omnidirectional waveheight estimates from the second-order energy were originally developed by [17]. This type of approach has been tested and validated for the phased-array OSCR HF radars by [21] and has been proven to provide reliable estimates of $Hs$. The use of information from overlapping stations provides two estimates of $Hs$ at each measurement location. The independent measurements can then be compared to estimate the reliability of the observations. No directional information can be obtained from a single radar alone without averaging over large azimuth angles, however by blending radar observations and models [22] estimated directional spectra from a single site.

The simple empirical approach was employed here to provide synoptic mapping of $Hs$. The waves and currents were simultaneously observed with the OSCR phased-array radar and *in situ* sensors during COPE–3. The accuracy of the remote observations as established by the *in situ* sensors is discussed in this paper in detail. The spatial variability of the near-surface currents and waveheights and the interaction between them during conditions when there was significant horizontal and vertical shear is then explored.

## II. COPE–3 Experiment

The OSCR system mapped surface currents and waveheights over the inner-shelf offshore the Chesapeake Bay mouth during the COPE–3 experiment in fall 1997 (Fig. 3). Vector current fields were obtained for the period from yearday (YD) 287 to YD 334. One station (HF–N) was located at the Fort Story, VA, U.S. Army base just to the south of the estuary mouth. The second radar station (HF–S) was located 18 km to the southeast at the U.S. Navy Fleet Combat Training Center Atlantic in Dam Neck, VA.

Both stations were operated at 25.4 MHz and transmitted a pulsed signal with a wavelength of 11.6 m. The corresponding ocean wave Bragg scattering wavelength was 5.8 m. This provided an estimate of the bulk-average of the currents over the top 0.4–1.5 m of the water column. The horizontal bin size was 1 km$^2$ over an area of approximately 30 km $\times$ 44 km (Fig. 3). There was a 5-min period of transmission at HF–S followed by 5 min at HF–N and then 10 min for processing the received signals. This sampling provided 468 pulses to produce the echo-Doppler spectrum from which the radial velocities were determined with an optimal accuracy of 0.02 m/s.

Estimates of $Hs$ were obtained at each measurement location through the ratio of the second-order backscattered energy to the first-order Bragg scattering energy following [17]. This empirical approach used linear scaling coefficients to minimize the mean square difference between HF radar observed and *in situ* $Hs$ measurements for $Hs>0.53$ m. The coefficients used to scale the second-order spectrum for this paper were calibrated from earlier OSCR measurements at Duck, NC [21].

Data from five acoustic Doppler current profilers (ADCP) were used in the validation studies (Fig. 3). The ADCPs were 307.2-kHz broadband "workhorse sentinels" manufactured by RD Instruments, San Diego, CA. They were deployed in bottom mounts in upward-looking configurations on October 6, 1997 (YD 279) and recovered on November 10, 1997 (YD 314). The vertical bin size was 1 m and valid currents were acquired from 2 m beneath the surface to about 4 m above the bottom. Water depths at the moorings ranged from 10 to 18 m. The sampling scheme used was a 1-min burst of 120 samples, which was repeated at 5-min intervals. Burst sampling was used to minimize aliasing of the measurement by surface gravity waves. Velocity data from each sample were resolved into northward and eastward components, then averaged over the burst. Raw data were further smoothed with a three-point running mean before analysis.

Wind and *in situ* wave measurements were obtained from the National Oceanic and Atmospheric Administration (NOAA) Coastal Marine Automated Network (CMAN) Chesapeake Bay Lighthouse Tower (CHLV2) station. The station was located within the HF radar measurement domain at a distance of 25 km from HF–N and 26 km from HF–S (Fig. 3). The anemometer was located at the top of the tower at a height of 43.3 m above the mean water level. Wind measurements were converted to standard 10-m height by assuming a log profile. The wind velocity and waveheight were recorded every 10 min throughout the experiment. The waveheight was derived from a laser height gauge mounted on the tower [23] and was nondirectional

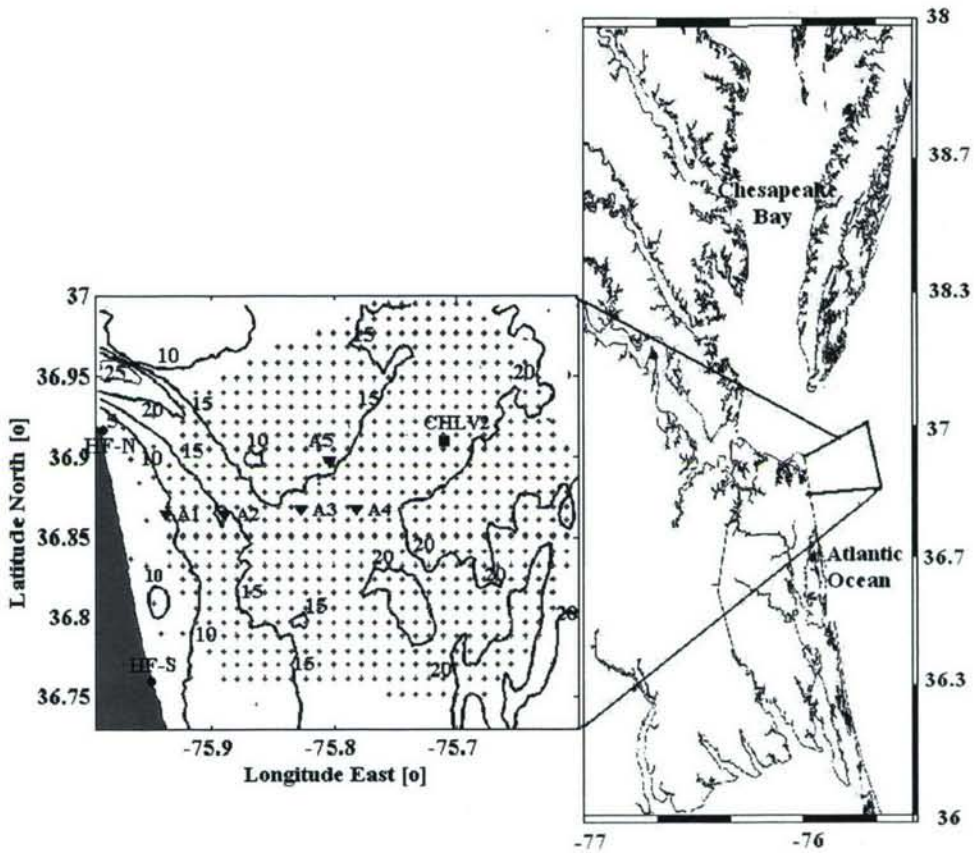


Fig. 3. Overview of Mid-Atlantic region (right). Topography and measurement locations for the COPE–3 experiment shown as inset. Depth contours are shown every 5 m. The center of each HF radar sample region is shown as (.). The shore stations are denoted by large solid circles. The ADCP moorings A1, A2, A3, A4, and A5 are shown with triangles. The CHLV2 CMAN station is shown as a square.

TABLE I
COMPARISONS OF OSCR HF RADAR CURRENT VELOCITIES WITH 2-m BIN OF ADCP. $\sigma$ IS THE STANDARD DEVIATION OF THE HF RADAR COMPONENT. $\Delta U$ AND $\Delta V$ ARE THE DIFFERENCES BETWEEN EAST–WEST AND NORTH–SOUTH COMPONENTS, RESPECTIVELY. CORRELATION SLOPE (m) AND BIAS (b) FOR EACH COMPONENT AS WELL AS THE COMPLEX CORRELATION COEFFICIENT ($\rho$) AND PHASE ($\varphi$) ARE SHOWN

| | U | | | | V | | | | | |
|---|---|---|---|---|---|---|---|---|---|---|
| | m/s | rms U m/s | m | b m/s | m/s | rms V m/s | m | b m/s | | |
| A2 | 0.25 | 0.11 | 1.1 | 0.05 | 0.31 | 0.10 | 0.9 | -0.02 | 0.94 | -9 |
| A3 | 0.22 | 0.09 | 1.0 | 0.02 | 0.21 | 0.09 | 1.1 | -0.02 | 0.91 | -4 |
| A4 | 0.18 | 0.07 | 1.0 | 0.02 | 0.19 | 0.08 | 1.2 | -0.01 | 0.90 | 2 |
| A5 | 0.16 | 0.07 | 1.1 | -0.01 | 0.21 | 0.10 | 1.2 | -0.02 | 0.94 | 12 |

## III. RESULTS

### A. Surface Current Comparisons With ADCPs

The East–West ($U$) and North–South ($V$) velocity components of each ADCP were compared with the nearest HF radar measurement. The HF radar $U$ velocities at A1 had unacceptably large errors because of the large angle between the two radials [11]. The results from this location were, therefore, omitted from the analysis. The second bin from the surface of the ADCP was used in each case because of the contamination of the first bin due to sidelobe reflections.

The statistics of the comparisons between the unfiltered OSCR observations in the near-surface layer and the ADCP revealed good agreement between the sensors (Table I). The slopes of the best fit regression curve were either 1.1 or 1 in each case for $U$ with biases below 0.05 m/s [24]. The slopes of the $V$ comparison ranged from 0.9 to 1.2 with biases between $-0.009$ m/s and $-0.018$ m/s. The complex correlation coefficient was 0.9 or above at each of the four moorings.

The rms difference between the HF radar and the ADCP $U$ component at A2 was larger than at the other moorings (0.11 m/s). This was in a region with large tidal excursions and this difference as a fraction of the velocity range was about

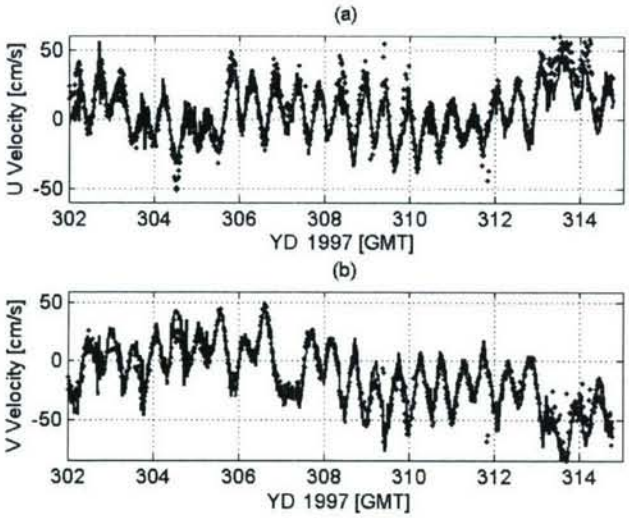


Fig. 4. Time series of unfiltered hourly surface (•, OSCR) and ADCP observed subsurface (solid) velocities at the A2 mooring. (a) $U$ (East–West) component positive toward east. (b) $V$ (North–South) component positive toward north.

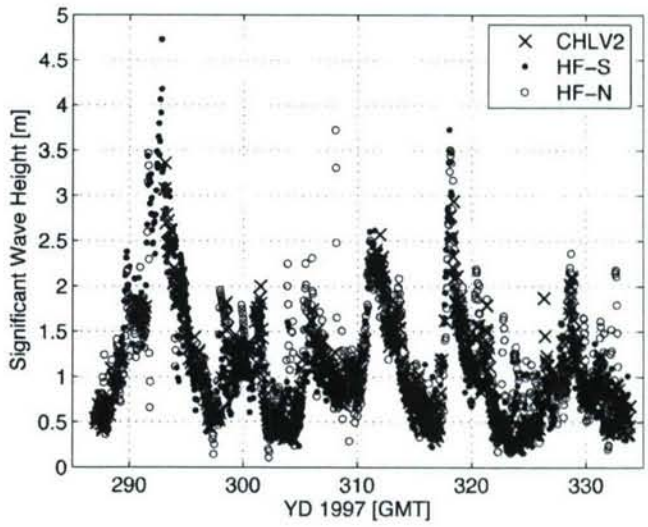


Fig. 5. Time series of the significant waveheight observed by HF radars HF–S (x), HF–N (+), and CHLV2 (•) tower mounted laser during the COPE–3 experiment in 1997.

11%. The time-series comparison of these velocities reveals the close relationship between the two measurements (Fig. 4). The only observable difference is that the OSCR $U$ observations were consistently larger than the ADCP values at the peak of the ebb tide and were intermittently larger at the peak of the flood tide. The amount of difference varied over each tidal cycle but was typically between 0.05 and 0.15 m/s.

### *B. Comparisons of HF Radar Waveheights With Laser Height Gauge*

The $Hs$ observed by HF–S and HF–N at the closest measurement cell were compared with those obtained at CHLV2. No adjustments to the scaling coefficients obtained from [21] were made to the values used here. The radar measurements track the passage of midlatitude fronts in a similar manner to CHLV2 (Fig. 5), although CHLV2 experienced data loss at the peak of the most energetic storms.

The largest waveheights during the experiment were recorded over the period from YD 291 to YD 295. The only measurement collected throughout this period was from HF–S. HF–S closely matched HF–N during the period before the peak and HF–S matched CHLV2 as the waveheight decreased.

On YD 312, both of the radars and CHLV2 recorded $Hs$ values between 2.5–2.8 m with the HF–S reading slightly higher than the other two. Later on YD 317, all three measurements again tracked the passage of a storm system with $Hs$ exceeding 3 m. In this case, both radars recorded peak values larger than CHLV2, but again there were dropouts in the laser measurements at the peak of the storm.

One-sided regressions revealed an rms difference of $Hs$ between HF–S and CHLV2 of 0.29 m (Table II). The rms difference between HF–N and CHLV2 was considerably larger (0.38 m) and it was 0.41 m between the two radar sites. The two-sided regressions produced smaller rms differences from 0.09 to 0.14 m in each case (Table II). Inspection of the scatter diagrams (Fig. 6) revealed that the main discrepancies were large values of $Hs$ recorded at HF–N when there were only small waves observed in the other two measurements [Fig. 6(b) and (c)]. The HF–N intermittently recorded $Hs$ values 0.5–1 m larger than HF–S and CHLV2 during periods with otherwise low waveheights. The large error at small waveheights in HF–N is reflected in percent relative error values exceeding 10% for waveheights less than 1 m [Fig. 6(d)]. The HF–S percent relative error did not exceed 10% except for waveheights less than 0.3 m [Fig. 6(d)].

The intermittent large HF–N observed $Hs$ values occurred most often between YD 303–YD 310 and from YD 320 to the end of the experiment. During the last period, the peaks occurred almost daily, but there was no consistent periodicity to their occurrence. The events of large $Hs$ at HF–N typically persisted for 2–4 h. The echo-Doppler spectrum recorded during these events contained large amounts of energy far removed from the Bragg peaks (Fig. 7). This indicated that outside signals contaminated the observations at these times. The HF–S observations did not have these short duration peaks except for a single event on YD 304.

The hourly radar wave observations from HF–S (767 900 points) were compared with the simultaneous current measurements at the same location. There was no correlation between the velocity magnitude (Vmag) or either of the components and the observed $Hs$ ($r = -0.03$, $-0.10$, and $-0.20$ for Vmag, $U$, and $V$). Similar correlation values were obtained with smaller subsets located near the CHLV2 tower and with the laser gauge. The slightly higher correlation with the $V$ component ($-0.2$) was related to the physical link between wind/wave forcing and this component of the currents.

The lack of correlation between the radar observations of $Hs$ and current velocity for the full data set demonstrated that the observed wave-current interaction during particular events was not an artifact of the radar measurement. This was expected because the two measurements were derived from the echo-Doppler spectrum in fundamentally distinct ways. The surface current was proportional to the displacement of the first-order

TABLE II
ONE-SIDED REGRESSIONS OF $Hs$ MEASUREMENTS FROM OSCR HF RADAR WITH CHLV2 CMAN OBSERVATIONS

| | rms diff. Hs (m) | Slope of best fit | Bias of best fit (m) |
|---|---|---|---|
| HF-N versus CHLV2 | 0.38 | 0.77 | 0.31 |
| HF-S versus CHLV2 | 0.29 | 0.80 | 0.14 |
| HF-N versus HF-S | 0.41 | 0.76 | 0.35 |

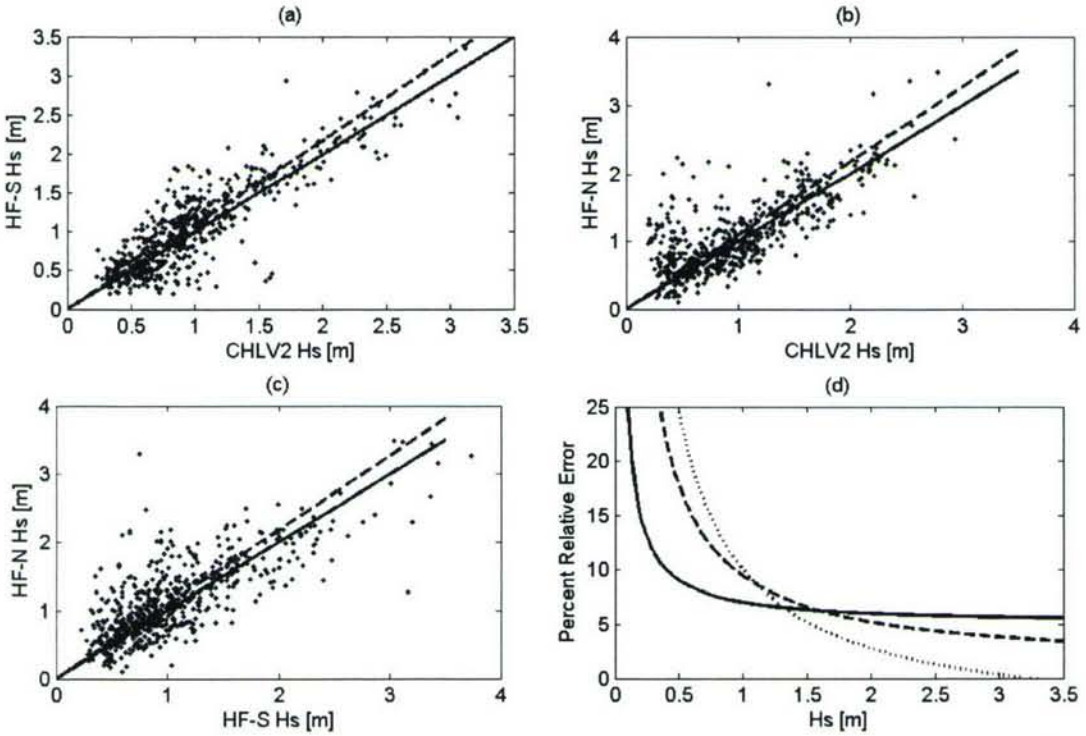


Fig. 6. (a) Significant waveheight as observed from the CHLV2 CMAN station versus the closest OSCR HF radar cell (♦) as observed from HF–S for the duration of COPE–3. Solid line is the unit slope line. Dashed line is the best fit two-sided regression. (b) Significant waveheight as observed from CHLV2 versus the closest OSCR HF radar cell (♦) as observed from HF–N for the duration of COPE–3. Solid line is the unit slope line. Dashed line is the slope of the best fit two-sided regression. (c) $Hs$ as observed from the HF–S versus the HF–N (♦). Solid line is the unit slope line, dashed line is the two-sided regression best fit. (d) Relative error percentage as a function of $Hs$. Solid line is CHLV2 versus HF–S. Dashed line is CHLV2 versus HF–N. Dotted line is HF–S versus HF–N.

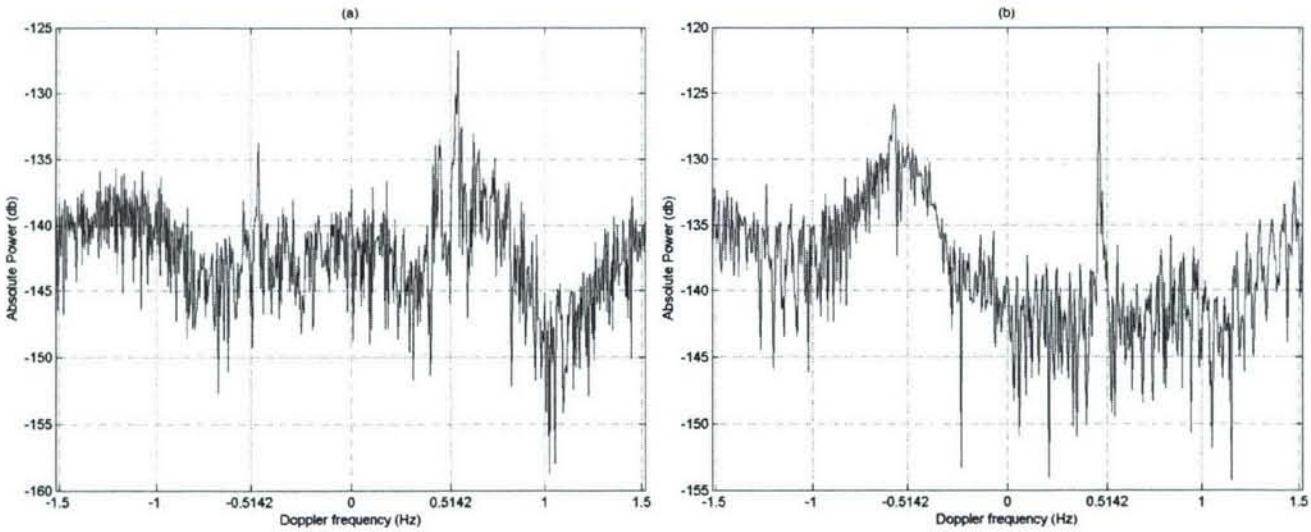


Fig. 7. Examples of large spurious signal in OSCR echo-Doppler spectra observed at HF–N during COPE–3 (a) YD 292.87 and (b) YD 290.96.

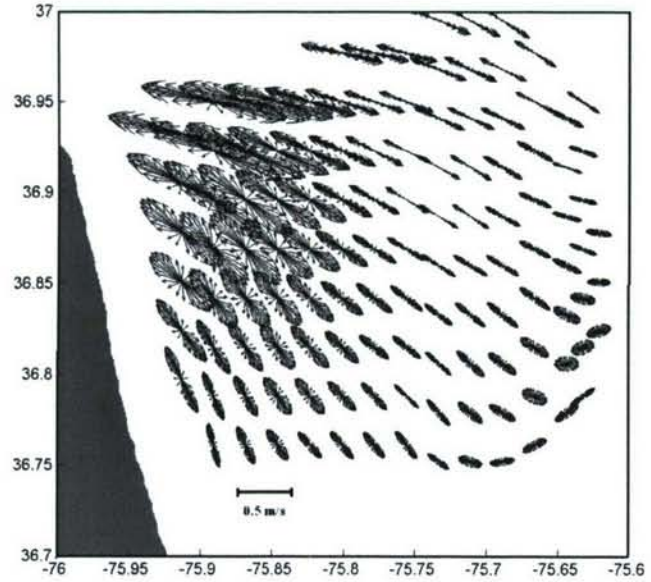


Fig. 8. Lunar semidiurnal (M2) tidal constituent ellipses derived from harmonic analysis of 45-d records of OSCR vectors during COPE–3. Horizontal axis—longitude East (decimal degrees). Vertical axis—latitude North (decimal degrees).

peaks in frequency space, while the $Hs$ was proportional to the ratio of the backscattered power in the second-order region to the first-order peak (Fig. 2).

### C. Tidal Currents

Analysis of the longest continuous segment of the COPE–3 surface current observations (35 d) confirmed that the lunar semidiurnal (M2) was the most energetic tidal component. There was little vertical structure of the M2 constituent (not shown) confirming that it was primarily barotropic [16]. The major axes of the M2 ellipses were generally aligned with the Chesapeake Bay mouth (Fig. 8). The strength of the M2 tide decreased with distance from the mouth. This decreasing velocity of the tidal flow with distance from the estuary mouth caused surface current convergences and divergences on particular phases of the tide.

During the ebb tide, the outflow of estuarine water from the Chesapeake Bay typically turned to the southeast and moved through the measurement domain. The highest surface velocities were usually associated with the ~20-m deep shipping channel in the northwest corner of the domain (Fig. 3). The buoyant plume associated with the estuarine outflow $w$ often formed a surface convergence front where it overrode denser shelf water.

### D. Waves Propagating Into Opposing Currents

As the ebb tide exited the bay mouth on YD 287.9, the wind was blowing from the southeast at 5.8 m/s. Under the assumption that the waves were propagating in the wind direction, this produced a situation in which the locally generated wind waves encountered a distinct surface current gradient (Fig. 9). Offshore the currents were weak (~0.15 m/s) and rotated to the right of the wind direction. In the region of the estuary mouth, the surface currents reached magnitudes over 1 m/s in opposition to the wind and wave direction.

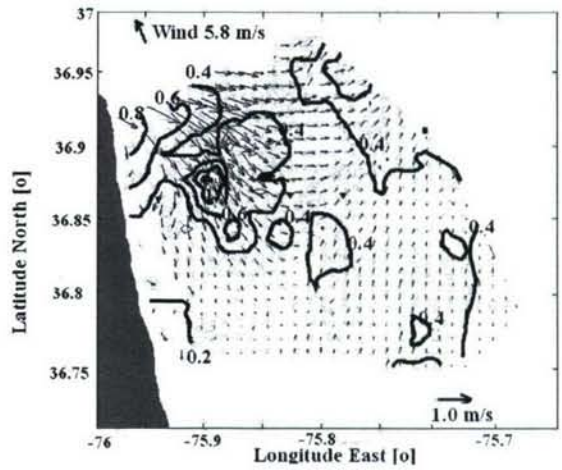


Fig. 9. Surface current (arrows, meter per second scale shown in lower right corner) vectors from combination of HF–S and HF–N radials and $Hs$ (contours, meter) as observed by HF–S on YD 287.78. Wind velocity at CHLV2 is shown in the upper left. Only those values obtained at ranges <= 26 km from HF–S are shown.

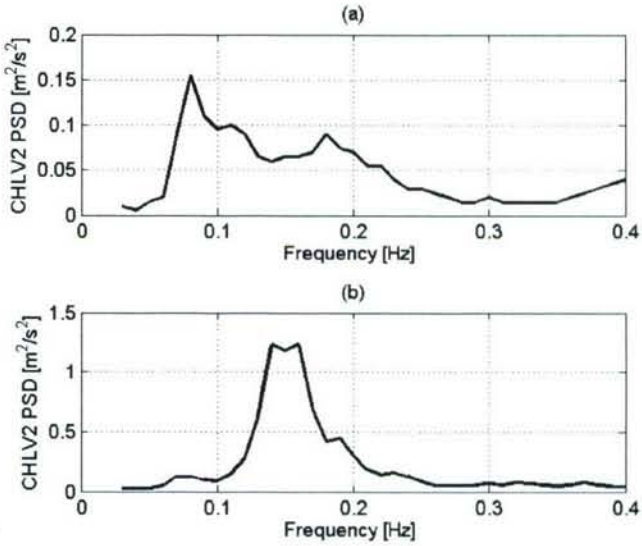


Fig. 10. Frequency spectra observed at CHLV2. (a) YD 287.78. (b) YD 305.33.

Over the southern half of the measurement domain, the HF–S-observed $Hs$ was generally <0.4 m (Fig. 9). $Hs$ increased to 0.6–0.8 m in the region of opposing currents near the A2 mooring. The largest $Hs$ values were associated with the strong outflow in the shipping channel that was directly in opposition to the wind/wave direction. In the center of the domain where the surface currents were directed more offshore, the $Hs$ values were less than 0.4 m. The frequency spectrum recorded at CHLV2 at this time revealed that in addition to the wind wave contribution around 0.17 Hz, there was a strong swell peak in the spectrum at 0.07 Hz Fig. 10(a). Inspection of the directional spectrum recorded 111 km east of the measurement region revealed that the swell was incident from a direction of 100°.

The wave shoaling derived from linear theory due to both the observed currents and topography was calculated over the entire

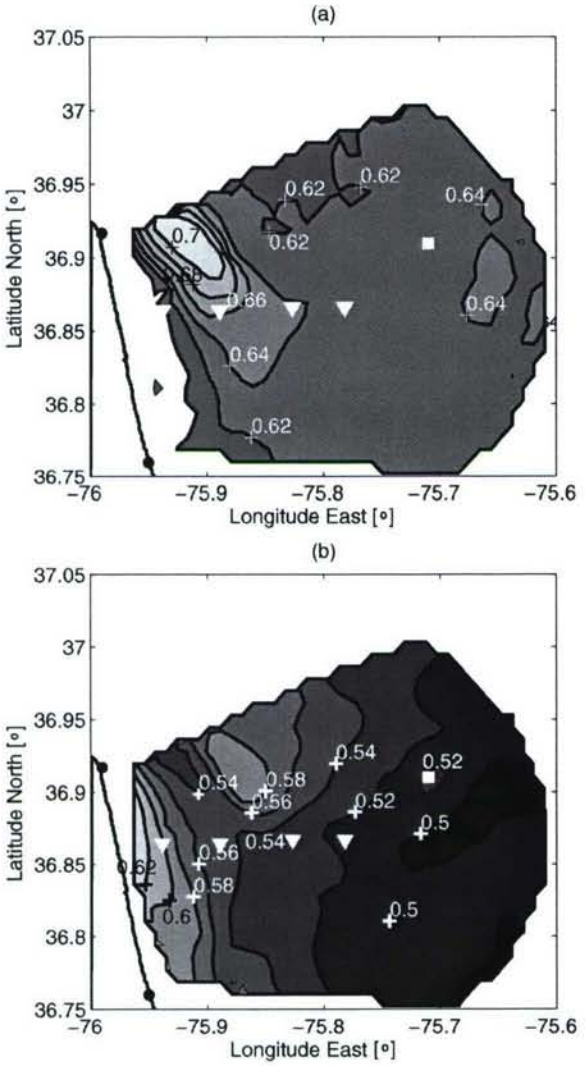


Fig. 11. $Hs$ (m) from linear theory shoaling due to topography and currents, assuming colinear waves and currents. $Hs$ contours shown every 0.02 m from 0.62 to 0.7 m. (a) Incoming waves from CHLV2 at 0.17 Hz in the wind direction 120°. (b) 0.07 Hz swell component with direction 100°. $Hs$ contours shown every 0.2 m from 0.5 to 0.62 m.

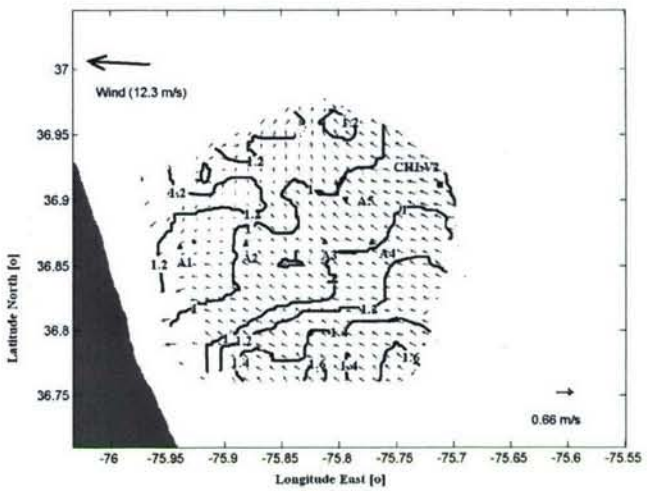


Fig. 12. $Hs$ (meter) and current velocities at peak of ebb tide on YD 305.33. Velocities determined by the combination of radials from each site. Velocity scale is in lower right corner. $Hs$ independently observed by HF–S. $Hs$ contours are given every 0.2 m; only values located <=26 km from HF–S shown.

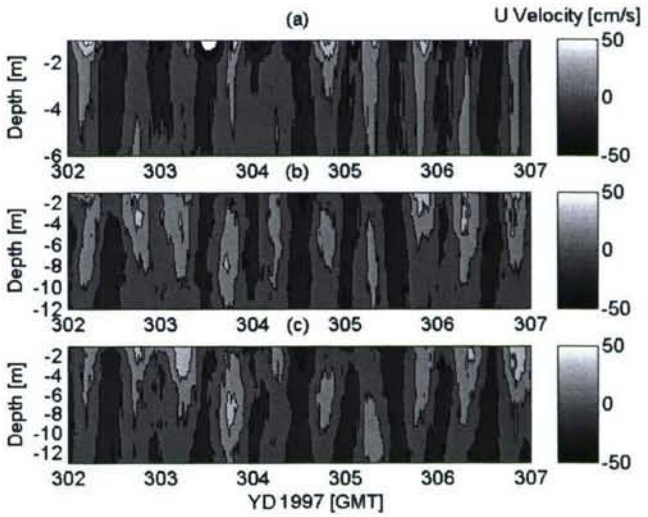


Fig. 13. $U$ component of the ADCP velocities during COPE–3 from YD 302 to YD 307. (a) A1. (b) A2. (c) A3. Negative $U$ denotes an onshore directed flow.

radar domain (Fig. 11) for both the wind wave and swell components. There was little influence of topography for the wind waves (0.17 Hz) because the depths were >5 m and the waves at this time were quite small. There was, however, a ~25% increase of $Hs$ due to the surface current. The radar results show the same order of effect localized to the region of the estuarine outflow. The swell wave (0.07 Hz) was not significantly influenced by the current, but was slightly enhanced over the shallower regions close to the shoreline and near the shoal in the center—north of the radar domain.

The winds during the period from 303.7 to 305.4 were consistently from the east or southeast but varied in magnitude from 5 to 12 m/s. On YD 305.33, the wind was 12.3 m/s in the onshore direction at the peak of the ebb tide. This caused the near-surface currents to be aligned in the wind direction over most of the domain Fig. 12. Near the mouth, the currents were much weaker or in the direction of the outgoing tide. At this time there was an increased $Hs$ observed in both radars near the estuary mouth Fig. 12. The frequency spectrum at CHLV2 revealed that the wind waves were dominant at this time [Fig. 10(b)] with the peak energy at 0.15 Hz.

There was significant vertical current shear southeast of the estuary mouth near the A1, A2, and A3 moorings. The vertical current profiles (Fig. 13) at these locations exhibited a surface layer velocity in the wind direction and a lower layer outflow. This was in contrast to the typical outflow at the peak of the ebb tide which was normally concentrated in the upper 5 m of the water column. At YD 304.7 and YD 305.3 at the peak of the ebb the outflow occurred in the middle of the water column. The near-surface layer velocities at these times were onshore in the direction of the wind forcing.

## IV. Discussion

### A. Validation of HF Radar Measurements With In Situ Sensors

The current velocities at the Chesapeake Bay mouth responded to the interaction between the tidal currents, buoyant discharge, wind forcing, and topography. The current response to wind forcing was further complicated by the disparate effects of the wind over the inner-shelf and within Chesapeake Bay. In particular, downwelling favorable winds over the shelf may produce a water level setup within the bay that drives a strong discharge at the mouth [25]. Comparisons of HF radar observations which were averaged over approximately 1 $km^2$ with point measurements were complicated by the high horizontal current shear. However, it was necessary to make these comparisons to evaluate the accuracy of the remote observations and to determine the spatial scales over which the point measurements were relevant.

The agreement between the HF radar current measurements and the near surface bin of the ADCPs was excellent throughout the experiment at moorings A2–A5. The HF radars and the ADCPs responded similarly to the range of currents observed (Fig. 4) with regression slopes close to 1.

The resolution of a radial velocity estimate was 0.022 m/s based on the pulse repetition rate and the sampling duration. The combination of the two radial components to estimate the vector velocity introduced additional error [11]. This error amplification was less than a factor of 2 (0.04 m/s), except for the North–South component at A4 and A5 and the East-West component at A1, where it reached a value of 2.5 (0.05 m/s).

The HF radars and ADCPs were operating within their expected accuracies. The rms differences for $U$ ranged from 0.068 to 0.113 m/s and, for $V$, they ranged from 0.079 to 0.101 m/s (Table I). These rms differences were of the same order as the 0.078 to 0.12 m/s observed by [26] and were less than the values of 0.112 to 0.158 m/s observed by [27], both of which used the same OSCR system as this paper. The *in situ* measurements for [26] were provided by moored instruments at depths of 4 m below the surface and, for [27], they were at a depth of 9.5 m. The deeper *in situ* depths relative to the 2-m ADCP upper bin used in this paper should have increased the contribution to the differences by Stokes drift and wind-induced shear [11]. These contributions totaled 0.025 m/s in [11] and this provides an indication of the strength of this effect in the current paper.

While baroclinicity can be very important in the region of the estuarine outflow, typical layer depths of the buoyant flow are ~5 m and its influence should be much larger at the inshore moorings. However, with the exception of the 0.046-m/s bias in $U$ at A2 the statistics of the comparisons are similar at all of the ADCPs. The biases at A3, A4, and A5 were <0.02 m/s for both components and the slopes ranged from 0.9 to 1.2 (Table I). These comparisons demonstrated the accuracy of the HF radar observation over much of the study region.

Two multifrequency coastal HF radars (MCR) and two SeaSonde HF radars also sampled the same general region during the COPE–3 experiment. The MCR was operated at frequencies of 4.8, 6.8, 13.4, and 21.8 MHz [28]. The SeaSonde was operated at a frequency of 25 MHz [29]. The most relevant MCR frequency for comparison with the OSCR was 21.8 MHz. The rms differences between the MCR at 21.8 MHz and the ADCP moorings were similar to those observed here (0.053–0.15 m/s). The MCR at A2 and A3 had larger rms differences than the OSCR when compared with the ADCP while the $V$ component offshore had lower rms differences. Because of the relatively small number of points used in the MCR comparison (103–403 samples) it is not possible to draw any firm conclusions about the generally small differences.

The rms differences between the SeaSonde radial velocities with antenna beam pattern corrections and the ADCP moorings ranged from 0.105 to 0.133 m/s [29]. These values were larger than the vector component rms differences observed by OSCR. Only radial SeaSonde comparisons have been published so it was not possible to discern how well the system as a whole was sampling the vector currents. Clearly, however, the errors can only increase when combining two nonorthogonal radial measurements. By spatially smoothing their results, the SeaSonde radial rms differences were reduced from 0.071 to 0.096 m/s which was of the same order as the OSCR vector component differences.

Both the MCR and the SeaSonde radial velocities were obtained with direction-finding algorithms corrected for measured antenna beam patterns. The OSCR phased-array results were not corrected for local perturbations to the antenna beam pattern. In spite of this, there was similar agreement between the three systems and the *in situ* currents. This demonstrated that the higher SNR obtained by the phased-array mitigated the need for antenna beam pattern corrections.

Inspection of the time series at A2 (Fig. 4) revealed that the differences between the HF radar and ADCP were not uniformly distributed relative to the phase of the M2 tide. The largest differences consistently occurred at the peak positive velocity (maximum ebb) and occasionally occurred at the peak negative velocity (maximum flood). These differences were typically ~0.10 m/s but on several occasions were ~0.20 m/s. These large differences at the peak ebb contributed significantly to the 0.046-m/s bias in the $U$ component as there was little increased surface velocity in the $V$ component and only a 0.018-m/s bias. These differences were also not observed at the other locations.

Previous studies have demonstrated that the M2 tide is primarily barotropic [16]. With the exception of frictional influences near the bottom it is, therefore, likely that local topography may have affected the comparison at this location. The A2 mooring was located at the inshore edge of the deep shipping channel leading into Chesapeake Bay (Fig. 3). At this mooring, the flow exhibited significant spatial variability particularly during a strong outflow (Fig. 9). The HF radar observed the velocity over a footprint that was nominally 1 km in horizontal extent. The cross-shelf scale of the convergence front of an estuarine outflow is typically an order of magnitude smaller than the HF radar resolution [30]. Because of this relatively large footprint, the HF radar observations may have included current velocities within the channel that were not observed at A2.

### B. Comparison of Wave Measurements From HF–N and HF–S

There are expected differences in the wave observations between the point measurement from the laser height gauge on

TABLE III
MEAN AND VARIANCE OF $Hs$ OBSERVATIONS

| Sensor | Samples | Mean Hs [m] | Var. Hs [m$^2$] |
|---|---|---|---|
| CHLV2 | 795 | 0.97 | 0.27 |
| HF–S | 1064 | 1.04 | 0.32 |
| HF–N | 898 | 1.09 | 0.29 |

CHLV2 and the spatially averaged observations from the radars. Comparisons are further complicated by the dropouts at CHLV2 at large $Hs$ and the spikes in the HF–N record at low $Hs$. The challenge was to intercompare these different types of observations and assess whether observed differences in wave parameters were statistically significant. Krogstad *et al.* [31] presented optimal regression methods to intercompare different types of wave measurements that are followed here for that purpose.

The most commonly applied statistical tests for intercomparison of measurements are one-sided regressions as done for the near-surface current measurements. The one-sided regressions between the radar-derived estimates and CHLV2 revealed that during the times when there were valid data, HF–S had better agreement than HF–N (Table II). In fact, HF–S agreed better with CHLV2 than with HF–N.

If the variances of the time series are similar as was the case in this paper (Table III), then it is more appropriate to perform a two-sided regression. The two-sided regressions through the origin have the same slope in all three cases [Fig. 6(a)–(c)]; however, it was clear that the comparisons of HF–N with the other two measurements contained larger rms differences (Table IV). The statistics of the comparison between HF–S and CHLV2 were within expected ranges based on the variability of the two systems. The comparison of HF–N to HF–S and CHLV2 revealed higher rms differences and a larger bias than has been observed in previous comparisons between *in situ* measurements [32]. The biases from the one-sided regression involving HF–N were also larger than those observed by [31] and [33] when comparing HF radar observations with *in situ* measurements. However, the two-sided regressions and ML estimates were similar to those reported in [32] (Table IV).

The maximum-likelihood (ML) approach as presented in [31] was used to determine how the sensor intercomparison varied with $Hs$. The percent relative error as a function of $Hs$ decayed for each of the comparisons [Fig. 6(d)]. However, there was much higher relative error at low waveheights for the cases involving HF–N. This resulted from the intermittent large spikes in the $Hs$ as observed from this station. For values of $Hs < 1$ m, the relative error of HF–N versus CHLV2 or HF–S increased rapidly from 10% to $> 25\%$ for $Hs < 0.5$ m.

For large waveheights, the relative error for the comparisons with CHLV2 remained at $>5\%$ while the HF–N to HF–S relative error decreased rapidly. This higher error was likely the result of the dropouts in the laser measurements at larger waveheights (Fig. 5). At the peak of the storm on YD 293 (October 20, 1997) the largest $Hs$ recorded by CHLV2 was 3.4 m while other National Data Buoy Center (NDBC) wave measurements north (buoy N44009) and south (DUCN7) of the station recorded values of 3.9 and 4.0 m, respectively. The NDBC buoy 60 nm offshore the measurement region (N44014) was not operating at the time of the storm. Furthermore, there was only one value above 3.5 m recorded at CHLV2 during the entire year of 1997. These factors demonstrate that the CHLV2 laser height sensor was not reliable for large waveheights ($Hs > 3$ m).

The time series (Fig. 5) of the three colocated $Hs$ measurements shows that the problems with HF–N were not systematic. Rather, there were frequent but intermittent periods in which HF–N overpredicted $Hs$. Inspection of the Doppler spectra at HF–N during the period when there were large differences between HF–N and HF–S and CHLV2 revealed large peaks at frequencies far removed from the Bragg peaks (Fig. 7). These spectra were not qualitatively similar to the normal spectral form (Fig. 2). Consequently, this and other techniques to extract the waveheight from the Doppler spectrum will fail. Because of the prevalence of the occurrence of these spurious spectra in the HF–N record, care must be taken to eliminate these values when interpreting the $Hs$ values obtained at this site.

The noise in the spectra observed at HF–N was likely caused by a local or directional source which was not observed in HF–S, or from a distant source that was more strongly coupled to the received signal at HF–N than HF–S because of the particular antenna characteristics at that site. Although it was not possible to determine precisely which phenomena was the cause here, it was likely that a local source was responsible. HF–N was located in close proximity ($\sim$300 m) to a U.S. Navy communication facility that intermittently used HF frequencies likely leading to the observed spurious signals. For this analysis, we will focus on the more reliable HF–S observations.

The comparison of the HF–S-derived $Hs$ with CHLV2 was encouraging for the purpose of mapping variability over the outflow plume. The 26-km range from HF–S to CHLV2 was near the practical limit of wave observations from the OSCR system [33]. This limitation is because the radar waveheight observations require the extraction of the energy in the second-order spectra (Fig. 2). With increasing range, the second-order signals are obscured by noise before the first-order peaks used to derive the radial currents. The plume frontal location varied considerably, but often a strong convergence front was present 10–20 km offshore HF–S. Therefore, the measurements in this region with better SNR than the comparison point should be quite reliable.

This empirical approach was surprisingly robust. The coefficients required to scale the linear relationship between the second-order power and $Hs$ were not determined locally. Rather, they were derived from an experiment three years earlier at Duck, NC, located $\sim$50 km south of the present study area. This demonstrated that the measurement was not highly sensitive to local perturbations to the antenna beam pattern. This gives confidence that HF–S-observed spatial variability of $Hs$ was real.

### C. Wave-Current Interaction

In light onshore winds and outgoing tide, enhanced waveheights were evident in the region of the main shipping channel (Fig. 9). When the wind forcing was light, locally generated waves were concentrated at high wave numbers. The frequency spectra recorded at CHLV2 on YD 287.78 revealed a large swell component at a frequency 0.07 Hz as well as the wind wave peak

TABLE IV
TWO-SIDED REGRESSION AND ML METHOD PARAMETERS FOR $Hs$ COMPARISON

| | rms difference Hs [m] | Two-sided regression slope | Bias of ML method [m] | Slope of ML method |
|---|---|---|---|---|
| HF-N versus CHLV2 | 0.26 | 1.09 | 0.08 | 1.01 |
| HF-S versus CHLV2 | 0.20 | 1.09 | 0.02 | 1.05 |
| HF-N versus HF-S | 0.27 | 1.09 | 0.15 | 0.96 |

at 0.17 Hz Fig. 10(a). On YD 305.33, the wind wave peak was significantly larger than any other component of the spectrum [Fig. 10(b)].

The wind waves were not sensitive to shoaling or refraction due to topography. They did not "feel" the bottom in our measurement domain because it did not get any shallower than ~5 m. Conversely, the influence of current velocity on these same waves was significant (Fig. 9), because the fraction of wave energy that was affected was higher at low winds (Fig. 1). The effects of nonlocal swell could be important in any wind regime, but would be more pronounced in light winds. Linear theory estimates of depth and current-influenced wave shoaling reveal a peak associated with the strong opposing current near the estuary mouth [Fig. 11(a)]. Estimates of the wave refraction (not shown) using ray theory showed no focusing of wave energy within the radar domain. Had the wind waves been obliquely incident to the current shear, then more refractive effects would have been observed.

The swell component (0.07 Hz) was expected to be less affected by the current Fig. 1 and more affected by the topography than the wind wave component. Linear theory estimates of the effect on the waveheight by both the current and topography predict a small enhancement of the waveheight over the shallower regions. However, because of the reduced effect of current on low-frequency waves there was no increased $Hs$ associated with the strong opposing current. There was some indication in the radar observations that the waveheight was increasing in the shallow region inshore of the strong outflow. This was consistent with shoaling of the swell component.

$Hs$ observations from HF–S on YD 305.33 were higher offshore the southeast portion of the domain, smaller in the center, and increased near the estuary mouth. The waveheights offshore the southeast were larger than elsewhere in the domain (Fig. 12). This was in a region where the depths were greater than 10 m and the tidal currents were weak. It was likely that the increased waveheights in this region resulted from the southeasterly winds that had been blowing earlier in the day. A southeast wind over the measurement region had unlimited fetch and, consequently, swell could have been propagating from this direction. Without local directional spectrum information however, this could not be established. In the middle of the domain, the waveheights were smallest. They then increased by 20–25% in the region southeast of the estuary mouth.

Weak near-surface currents on YD 305.33 opposed the wave propagation in the region of increased $Hs$. They averaged 20 cm/s less than the currents in the wind direction farther offshore. Since this was the peak of the ebb tide, it was likely that the wind-forced near-surface currents were interacting with the normally barotropic [16] M2 tidal outflow. Inspection of the ADCP profiles at the A2 and A3 moorings revealed that the vertical structure of the tidal flow changed during the period of strong onshore winds (Fig. 13). The offshore flow at the peak of ebb tides both before and after this period was strongest in the upper 5 m. However, from YD 304.5 to 305.5, the peak ebb tidal velocities shifted deeper in the water column and there was onshore flow in the near-surface layer. Unfortunately, salinity and temperature profiles were not available at this time; however, it is likely that this was an unstable situation with denser shelf water being forced over the outgoing estuarine flow. This region then would have been undergoing significant mixing, particularly given the relatively large waveheights.

The waveheights were reduced where the surface layer was moving in the wind direction (Fig. 11). Kirby and Chen [34] derived a hyperbolically decaying expression for the equivalent current velocity for a depth-varying current at a given wave number. For the wave numbers present at this time Fig. 10(b), their expression predicted little influence of the observed currents on the waves. Our observations were consistent with [34] in that it was only near the estuary mouth and close to shore where the surface currents were opposing the wind direction [Figs. 11 and 13(c)] that enhanced waveheights were observed.

For most users of near-real time wave information, it is not necessary to describe the surface waves in great detail. Rather, significant waveheights and mean directions are most likely to be of primary interest. It is clear from the results presented here that phased-array radars can provide information on the spatial variability of $Hs$. This could be of significant interest in locations such as the study area where strong currents can lead to locally enhanced $Hs$. The difference between an $Hs$ of 1.4 and 2.0 m over a few kilometers [Fig. 11(a)] may be significant for safe operation of small vessels. With the position of the outflow plume highly dependent upon the discharge, tide stage, and wind [35], it is not possible for a few point measurements to adequately sample the spatial variability of $Hs$ over the outflow plume. Since the $Hs$ estimates from the radars are empirically based, it is necessary, however, to have at least one reliable *in situ* wave observation for calibration and verification purposes.

To establish a predictive capability for the local wave conditions, it is necessary to implement linked shallow-water cir-

culation and wave models. Such an approach would be greatly enhanced by the observation of the wave directional spectra as in [33]. Given the requirement for *in situ* calibration and long-term observation over a range of wind and current conditions and the considerable expense associated with these efforts, it is clear that the necessary information to extract the full directional spectrum from phased-array systems should be retained whenever possible.

## V. Summary

Surface currents and significant waveheights have been successfully observed with an HF radar system deployed near the mouth of the Chesapeake Bay. The remotely sensed currents and waves were compared with *in situ* observations using ADCPs and a laser height gauge, respectively. The agreement between the HF radar observed near-surface currents and the near-surface bin of the ADCPs was very good throughout the experiment. Observed differences were similar to or less than previous comparisons between HF-radar-derived velocities and *in situ* point measurements. In particular, the vector component differences were of the same order as beam pattern corrected radial differences from a direction-finding system deployed during the same experiment. This demonstrated that antenna beam pattern corrections were not necessary for obtaining reliable surface currents from the phased-array system.

Comparison of radar $Hs$ measurements with an *in situ* laser revealed differences of the same order as in earlier studies. Although there were conditions under which one of the radar units estimated erroneously large $Hs$, the slope of the regression between the wave observations was only 1.09. These intermittent large values resulted from broad spurious peaks in the echo-Doppler spectrum which could be removed *a priori*. Given that the comparisons were made near the practical range limit (25 km) of wave observations with the OSCR, the agreement with *in situ* point observations provided confidence that the observed spatial structure of $Hs$ was valid.

The combined wave and current information over this tidally dominated region with complex topography revealed regions with significant wave-current interaction. There were several occasions during the 45 d of the experiment when the incident waves were propagating into an opposing current. The waveheights in low-moderate winds increased by 25%–50% above incident values, which was comparable to linear theory estimates. When there was stronger wind forcing, the near-surface currents were directed with the wind, while the tidal outflow currents below 3 m were in opposition to the wind direction. This probably caused substantial mixing between estuary and shelf water.

Real-time dissemination of the locations where waves are enhanced could improve the safety of commercial and recreational maritime activities. Longer term measurements and additional comparisons with models for wave refraction and diffraction in coastal regions will be necessary to quantify the effects of opposing currents on the wave field over a range of conditions. Also, derivation of the full directional wave spectrum from phased-array radar measurements would provide more comprehensive information. This could then be incorporated into regional wave and circulation models to develop a predictive capability.

## Acknowledgment

The authors would like to thank the personnel of the U.S. Army base at Fort Story, VA and the U.S. Navy Fleet Combat Training Center Atlantic for the use of their facilities as ground stations for the HF radar antennas. They would also like to thank J. Martinez, M. Rebozo, T. Cook, S. Nikolic, and T. Faber of the University of Miami, Coral Gables, for their diligent work during the experiment.

## References

[1] O. S. Shemdin, V. Hsiao, H. E. Carlson, K. Hasselmann, and K. Schulze, "Mechanisms of wave transformation in finite depth water," *J. Geophys. Res.*, pp. 85 5012–85 5018, 1980.

[2] R. Dean and R. A. Dalrymple, *Water Wave Mechanics for Engineers and Scientists*. Singapore: World Scientific, 1991.

[3] C. C. Mei, *The Applied Dynamics of Ocean Surface Waves*. Singapore: World Scientific, 1989.

[4] K. Kenyon, "Wave refraction in ocean currents," *Deep Sea Res.*, vol. 18, pp. 1023–1034, 1971.

[5] J. T. Kirby and R. A. Dalrymple, "A parabolic equation for the combined refraction-diffraction of Stokes waves by mildly varying topography," *J. Fluid Mech.*, vol. 136, pp. 543–566, 1983.

[6] C. L. Vincent and M. J. Briggs, "Refraction-diffraction of irregular waves over a mound," *J. Waterway, Port Coastal, Ocean Eng.*, vol. 115, pp. 269–284, 1989.

[7] S. P. Kingsley, T. M. Blake, T. M. Fisher, A. J. Ledgard, and L. R. Wyatt, "Dual HF radar measurements of sea waves from straight coastlines," in *Proc. IEEE Conf. HF Radio Syst. Tech.*, 1997, pp. 330–333, No. 411.

[8] B. K. Haus, J. D. Wang, J. Martinez-Pedraja, and N. Smith, "Southeast Florida shelf circulation and volume exchange, observations of km-scale variability," *Estuarine Coastal Shelf Sci.*, vol. 59, no. 2, pp. 277–294, 2004.

[9] D. E. Barrick and B. J. Lipa, "An evaluation of least-squares and closed-form dual-angle methods for CODAR surface-current applications," *IEEE J. Ocean. Eng.*, vol. OE-11, no. 2, pp. 322–326, Apr. 1986.

[10] R. H. Stewart and J. W. Joy, "HF radio measurements of surface currents," *Deep Sea Res.*, vol. 23, pp. 1039–1049, 1974.

[11] H. C. Graber, B. K. Haus, L. K. Shay, and R. D. Chapman, "HF radar comparisons with moored estimates of current speed and direction: Expected differences and implications," *J. Geophys. Res.*, vol. 102, pp. 18 749–18 766, 1997.

[12] D. Prandle, "A new view of near-shore dynamics based on observations from HF radar," *Prog. Oceanogr.*, vol. 27, pp. 403–438, 1989.

[13] B. K. Haus, J. D. Wang, J. Rivera, N. Smith, and J. Martinez-Pedraja, "Remote radar measurement of shelf currents off Key Largo, Florida," *Estuarine, Coastal Shelf Sci.*, vol. 51, pp. 553–569, 2000.

[14] B. K. Haus, H. C. Graber, L. K. Shay, and T. M. Cook, "Alongshelf variability of a coastal buoyancy current during the relaxation of downwelling favorable winds," *J. Coastal Res.*, vol. 19, no. 2, pp. 409–420, 2003.

[15] G. O. Marmorino, L. K. Shay, B. K. Haus, R. A. Handler, H. Graber, and M. P. Horne, "An EOF analysis of HF Doppler radar current measurements of the Chesapeake Bay buoyant outflow," *Cont. Shelf Res.*, vol. 19, pp. 271–288, 1999.

[16] L. K. Shay, T. M. Cook, B. K. Haus, H. C. Graber, J. Martinez, and Z. R. Hallock, "The strength of the M2 tide at the mouth of the Chesapeake Bay," *J. Phys. Oceanogr.*, vol. 31, pp. 427–449, 2001.

[17] D. E. Barrick, "Extraction of wave parameters from measured HF radar sea-echo Doppler spectra," *Radio Sci.*, vol. 12, no. 3, pp. 415–424, 1977.

[18] R. Howell and J. Walsh, "Measurement of ocean wave spectra using narrow-beam HF radar," *J. Ocean. Eng.*, vol. 18, no. 3, pp. 296–305, Jul. 1993.

[19] L. R. Wyatt, "A relaxation method for integral inversion applied to HF radar measurement of the ocean wave directional spectrum," *Int. J. Remote Sens.*, vol. 11, pp. 1481–1494, 1990.

[20] L. R. Wyatt, S. P. Thompson, and R. R. Burton, "Evaluation of high frequency radar wave measurement," *Coastal Eng.*, vol. 37, pp. 259–282, 1999.

[21] H. C. Graber and M. L. Heron, "Wave height measurements from HF radar," *Oceanography*, vol. 10, no. 2, pp. 90–92, 1997.
[22] C. de Valk, A. Reniers, J. Atanga, A. Vizinho, and J. Vogelzang, "Monitoring surface waves in coastal waters by integrating HF radar measurement and modeling," *J. Coastal Eng.*, vol. 37, pp. 431–453, 1999.
[23] C. C. Teng, "Wave measurements from NDBC buoys and CMAN stations," in *Proc. MTS/IEEE Conf. OCEANS*, 2002, pp. 517–524.
[24] L. K. Shay, T. M. Cook, B. K. Haus, H. C. Graber, J. Martinez, and Z. R. Hallock, "Observed surface currents during the Chesapeake Bay outflow plume experiments," in *Proc. 1st Int. Workshop Radiowave Oceanogr.*, Miami, FL, 2003, pp. 137–145.
[25] A. Valle-Levinson, C. Li, T. C. Royer, and L. P. Atkinson, "Flow patterns at the Chesapeake Bay entrance," *Cont. Shelf Res.*, vol. 18, pp. 1157–1177, 1998.
[26] L. K. Shay, S. J. Lentz, H. C. Graber, and B. K. Haus, "Current structure variations detected by high-frequency radar and vector-measuring current meters," *J. Phys. Oceanogr.*, vol. 15, pp. 237–256, 1998.
[27] L. K. Shay, H. C. Graber, D. B. Ross, and R. D. Chapman, "Mesoscale ocean surface current structure detected by HF radar," *J. Atmos. Ocean. Technol.*, vol. 12, pp. 881–900, 1995.
[28] C. C. Teague, J. F. Vesecky, and Z. R. Hallock, "A comparison of multifrequency HF radar and ADCP measurements of near-surface currents during COPE-3," *IEEE J. Ocean. Eng.*, vol. 26, no. 3, pp. 399–405, Jul. 2001.
[29] J. Paduan, D. Barrick, D. Fernandez, Z. R. Hallock, and C. Teague, "Improving the accuracy of coastal HF radar current mapping," *Hydro Int.*, vol. 5, no. 1, pp. 1–5, 2001.
[30] J. O'Donnel and G. O. Marmorino, "Convergence and downwelling at a river plume front," *J. Phys. Oceanogr.*, vol. 28, pp. 1481–1495, 1998.
[31] H. E. Krogstad, J. Wolf, S. P. Thompson, and L. R. Wyatt, "Methods for intercomparison of wave measurements," *Coastal Eng.*, vol. 37, pp. 235–257, 1999.
[32] H. C. Graber, E. A. Terray, M. A. Donelan, W. M. Drennan, J. C. Van Leer, and D. B. Peters, "ASIS-a new air-sea interaction spar buoy: Design and performance at sea," *J. Atmos. Ocean. Technol.*, vol. 17, no. 5, pp. 708–720, 2000.
[33] L. R. Wyatt, G. Liakhovetski, H. C. Graber, and B. K. Haus, "Factors affecting the accuracy of Showex HF radar wave measurements," *J. Atmos. Ocean. Technol.*, vol. 22, pp. 847–859, 2005.
[34] J. T. Kirby and T.-M. Chen, "Surface waves on vertically sheared flows: Approximate dispersion relations," *J. Geophys. Res.*, vol. 94, no. 1, pp. 1013–1027, 1989.
[35] Z. R. Hallock and G. O. Marmorino, "Observations of the response of a buoyant estuarine plume to upwelling favorable winds," *J. Geophys. Res.*, vol. 107, no. C7, 2002, doi: 10.1029/2000JC000698.
[36] M. A. Donelan, M. Skafel, H. C. Graber, P. Liu, D. Schwab, and S. Venkatesh, "On the growth rate of wind-generated waves," *Atmos.—Ocean*, vol. 30, no. 3, pp. 457–478, 1992.

**Brian K. Haus** (M'04) was born in Midland, MI, in 1964. He received the B.S., M.S.E., and Ph.D. degrees from the University of Michigan, Ann Arbor, in 1987, 1989, and 1992, respectively. His graduate work was in coastal engineering within the Naval Architecture and Marine Engineering Department.

Since 1993, he has been with the Division of Applied Marine Physics at the Rosenstiel School of Marine and Atmospheric Science, University of Miami, Miami, where he now is a Research Associate Professor. He has been the Manager of the Air–Sea Interaction Saltwater Tank (ASIST) since its inception. His work in ASIST involves optical and radar measurements of the air–sea interface under strong wind forcing and wave-current interaction studies. He has deployed phased-array HF radar systems at many locations along the United States Atlantic coast. Currently, he is studying application of the WEllen RAdar (WERA) HF radar system for combined wave and current measurements through it use in the southeast Atlantic coastal ocean observing system. His primary research interests include HF radar oceanography, coastal circulation, air–sea interaction studies, and wave-current interaction.

**Rafael J. Ramos** was born in Mexico City, Mexico, in 1967. He received the B.Sc. degree in civil engineering from Instituto Politecnico Nacional, Mexico City, Mexico, in 1989, the M.S. degree in ocean engineering from Texas A&M University, College Station, in 1995, working on the estimation of the response of floating structures due to wave loading, and the Ph.D. degree working on sampling ocean properties with HF radar at the Rosenstiel School of Marine and Atmospheric Science, University of Miami, Miami, in 2006.

He joined Instituto Mexicano del Petroleo (IMP), Mexico, where he participated in several projects involving the determination of environmental loading and the structural response of offshore platforms in the Gulf of Mexico. In 1997, he was appointed Head of the Offshore Platform Engineering Research Group. He lead several projects involving monitoring, risk assessment, and regulation of offshore platforms and pipelines in Bay of Campeche in collaboration with the University of California at Berkeley, the U.S. Minerals Management Service, and other research and engineering groups. He is currently with the Center for Southeastern Tropical Advanced Remote Sensing, University of Miami.

**Hans C. Graber** received the B.E. degree in civil engineering from the City College of New York (CCNY), New York, in 1977 and the M.S. and Sc.D. degrees in hydrodynamics from the Massachusetts Institute of Technology (MIT), Cambridge, in 1979 and 1984, respectively.

He is currently a Professor in the Division of Applied Marine Physics, Rosenstiel School of Marine and Atmospheric Science, University of Miami, Miami, FL, and also serves as Co-Director of the University of Miami's Center for Southeastern Tropical Advanced Remote Sensing (CSTARS). He is Co-Chair of the Radio Oceanography Workshop (ROW) and Waves in Shallow-Water Environment (WISE). For many years, he led the HF radar technology effort at the University of Miami which included numerous experiments such as High-resolution Remote Sensing Experiment (HIRES), DUCK94, COPE–1, and COPE–3 as well as Shoaling Waves Experiment (SHOWEX). He led the development of the Air–Sea Interaction Spar buoy and participated in numerous sea-going air–sea interaction experiments such as Office of Naval Research's Surface Wave Dynamics Experiment (SWADE), HIRES, and SHOWEX. He is the lead Principal Investigator of a multipartnership National Oceanographic Partnership Program (NOPP) team on Real Time Forecasting of Winds, Waves, and Surge in Tropical Cyclones. He has been a member on National Aeronautics and Space Administration's (NASA's) Scientific Working Group for NASA scatterometer (NSCAT) and on the Ocean Vector Wind Science Team for Seawinds and served on several European Union and Commission Expert Review Boards. His research interests focus on experimental, theoretical, and numerical investigations of the ocean surface wave dynamics, radar remote sensing, air–sea fluxes including boundary-layer dynamics, and hurricane and storm surge predictions.

Dr. Graber served as Guest Editor of the *Oceanography* magazine special issue on "HF Radar for Coastal Oceanography" and as Editor for the Oceanic Section of the *AMS Journal of Atmospheric and Oceanographic Technology*.

**Lynn K. Shay** received the B.S. degree from the Florida Institute of Technology, Melbourne, in 1976 and the M.S. and Ph.D. degrees from the U.S. Naval Postgraduate School, Monterey, CA, in 1983 and 1987, respectively, all in physical oceanography.

He is currently a Professor in the Division of Meteorology and Physical Oceanography at the Rosenstiel School of Marine and Atmospheric Science, University of Miami, Miami, FL. He has participated in a broad spectrum of field programs including the ONR/NASA Surface Wave Dynamics Experiment, NSF/NOAA Hurricane Air–Sea Interaction Experiments in Gordon, Michelle, Isidore, Lili, Katrina, and Rita, ONR High Resolution Remote Sensing Experiments, Chesapeake Bay Outflow Plume Experiments, 4-D Current Experiment, Adverse Weather Experiment using the Ocean Surface Current Radar, and more recently the West Florida Shelf and East Florida Shelf HF Radar Testbed Experiments using a Wellen Radar as part of the SouthEast

Atlantic Coastal Ocean Observing System. He was the Lead Oceanographer on the aircraft part of the NSF/NOAA Eastern Pacific Investigation of Climate. He has authored and coauthored over a hundred peer-reviewed manuscripts and reports. His research interests include experimental and theoretical investigations of the ocean response and coupled air–sea interactions during strong forcing events such as hurricanes, airborne oceanographic profiling of upper ocean (including the surface mixed layer) variability, coastal oceanographic process studies, and high-frequency (HF) and satellite radar remote sensing to examine the linkages between surface processes and oceanic structures.

Dr. Shay is a NOAA Cooperative Institute of Marine and Atmospheric Science Fellow, a Member of the American Meteorological Society's Tropical Meteorology and Tropical Cyclones Committee, a Member of the Ocean.US Surface Current Mapping Initiative team, a Member of the American Geophysical Union and Oceanography Society, and a Member of the Editorial Board of Elsevier's *Dynamics and Atmospheres and Oceans* journal. He Co-Chaired the NSF/NOAA prospectus Development Team Hurricanes at Landfall committee. He serves as Co-Chief Editor of the *AMS Journal of Atmospheric and Oceanographic Technology-Oceans*.

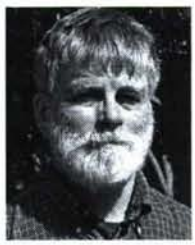

**Zachariah R. Hallock** received the B.S. degree in physics from the Polytechnic Institute of Brooklyn, NY, in 1970 and the M.S. and Ph.D. degrees in physical oceanography from the Rosenstiel School of Marine and Atmospheric Science, University of Miami, Miami, in 1973 and 1977, respectively.

He then joined the U.S. Naval Oceanographic Office where he planned and conducted large-scale oceanographic surveys in areas of Navy interest. In 1981, he transferred to the Oceanography Division of the Naval Research Laboratory (then NORDA) where he initially conducted research in oceanic thermohaline fine structure using observations from frontal regions. In 1985, he pursued research in oceanic mesoscale variability in multidisciplinary programs. This work included field observations and analyses of moored and profile measurements in combination with satellite altimetry and model results. In 1990, he began a study of deep boundary flows in the northwest Pacific near Japan, in collaboration with concurrent Naval Research Laboratory (NRL) remote sensing and modeling efforts. His most recent research focused on coastal oceanic processes including tidal studies, oceanic fronts, and internal wave effects on acoustics. He is now retired from NRL and maintains an office at home in Efland, NC.

Dr. Hallock is a Member of the American Geophysical Union and Sigma Xi.